HHS Public Access

Author manuscript

Plast Reconstr Surg. Author manuscript; available in PMC 2020 December 01.

Published in final edited form as:

Plast Reconstr Surg. 2019 December ; 144(6): 1051e–1060e. doi:10.1097/PRS.0000000000006260.

"Quantification of head shape from three-dimensional photography for pre- and post-surgical evaluation of craniosynostosis"

Antonio R. Porras, PhD[1], **Tu Liyun, PhD**[1], **Deki Tsering**[2], **Esperanza Mantilla, MD**[3], **Albert Oh, MD**[3], **Andinet Enquobahrie, PhD**[4], **Robert Keating, MD**[2], **Gary F. Rogers, MD**[3], **Marius George Linguraru, DPhil**[1,5]

[1]Sheikh Zayed Institute for Pediatric Surgical Innovation – Children's National Health System. Washington, DC, 20010, USA

[2]Department of Neurosurgery - Children's National Health System. Washington, DC, 20010, USA

[3]Department of Plastic and Reconstructive Surgery - Children's National Health System. Washington, DC, 20010, USA

[4]Kitware Inc. Carrboro, NC, 27510, USA

[5]Departments of Radiology, Pediatrics and Biomedical Engineering, George Washington University, Washington, DC, 20037, USA

Abstract

Background: Evaluation of surgical treatment for craniosynostosis is typically based on subjective visual assessment or simple clinical metrics of cranial shape that are prone to inter-observer variability. 3D photography provides cheap and non-invasive information to assess surgical outcomes, but there are no clinical tools to analyze it. We aim to objectively and automatically quantify head shape from 3D photography.

Methods: We present an automatic method to quantify intuitive metrics of local head shape from 3D photography using a normative statistical head shape model built from 201 subjects. We use these metrics together with a machine learning classifier to distinguish between patients with (N=266) and without (N=201) craniosynostosis (age: 0-6 years). We also use our algorithms to quantify objectively local surgical head shape improvements on 18 patients with pre- and post-surgical 3D photographs.

Results: Our methods detected craniosynostosis automatically with 94.74% sensitivity and 96.02% specificity. Within the dataset of patients with craniosynostosis, we identified correctly the fused sutures with 99.51% sensitivity and 99.13% specificity. When we compared quantitatively the pre- and post-surgical head shapes of patients with craniosynostosis, we obtained a significant reduction of head shape abnormalities ($p<5\%$), in agreement with the treatment approach and the clinical observations.

Corresponding author: Antonio R. Porras, PhD., Address: Sheikh Zayed Institute for Pediatric Surgical Innovation – Children's National Health System. Office M7735, 111 Michigan Ave NW, Washington, DC, 20009. aporraspe@childrensnational.org.

Conclusions: Quantitative head shape analysis and 3D photography provide an accurate and objective tool to screen for head shape abnormalities at low cost and avoiding imaging with radiation and/or sedation. Our automatic quantitative framework allows for the evaluation of surgical outcomes and has the potential to detect relapses.

Introduction

Craniosynostosis affects 1 in 2,100-2,500 live births[1,2] and its most common presentation are cranial malformations in the first year of life[3]. The condition often involves intra-cranial pressure and impaired brain growth. Three-dimensional (3D) computed tomography (CT) is the de facto imaging standard to diagnose craniosynostosis based on the observation of the fused sutures[4,5] and to plan surgical correction. Due to concerns about exposing children to harmful radiation and sometimes sedation, post-surgical CT images are normally avoided unless suboptimal treatment or relapse are suspected.

During the last few years, 3D photography has gained popularity as a non-invasive and inexpensive technology to evaluate the head shape of these patients. However, unlike CT images, 3D photographs do not provide visualization of the cranial bones and sutures. In this work, we present a novel methodology to quantitatively evaluate the head shape from 3D photography for the objective detection of abnormalities caused by craniosynostosis. Our approach can effectively evaluate surgical results.

State of the art

Traditional quantification of head shape abnormalities is based on three clinical metrics: head circumference, cephalic index and intra-cranial volume. The American Academy of Pediatrics recommends all children to undergo standard routine head circumference measurements, but this metric has shown low reliability, high inter-observer variability, and low sensitivity to detect craniosynostosis[6–8]. Although the cephalic index is often used to evaluate patients with sagittal craniosynostosis, it is not discriminative in patients with other types of craniosynostosis and a high number of patients with sagittal suture fusion present normal cephalic indices[9,10]. The intra-cranial volume, on the other hand, has been largely used to evaluate cranial growth, but it requires CT or magnetic resonance (MR) images for its calculation. Moreover, studies have shown that children with craniosynostosis often have intra-cranial volumes in normal ranges[11–13].

In our previous work[5], we showed that the quantification of local cranial bone abnormalities from CT images using a normative statistical cranial bone shape model can detect craniosynostosis with 93% sensitivity. In addition, we used that quantitative framework to create the optimal surgical plan personalized to each patient[14]. However, despite the potential of that technology to introduce objectivity in the clinical management of patients with craniosynostosis, its application to post-surgical assessment or longitudinal evaluation is limited, since CT image are not routinely acquired after surgery to avoid exposing children to unnecessary radiation.

Recent studies have shown the potential of 3D photography to evaluate the surgical outcome of patients with craniosynostosis non-invasively and at a lower cost than CT or MR. For

example, Tenhagen et al.[15] used hand-held 3D photographs to compare the cephalic index, head circumference, volume, sagittal length, and coronal width of patients with sagittal craniosynostosis before and after surgery. Rodriguez-Florez et al.[16] used Principal Component Analysis (PCA) on hand-held 3D photographs to evaluate forehead variations between the pre- and post-surgical shapes of patients with trigonocephaly. Meulstee et al.[17] used PCA to calculate the principal modes of head shape variations in healthy patients and identified significant differences in patients with scaphocephaly and trigonocephaly. However, they did not provide a solution to quantify the degree of head malformations and their exact location, and they did not study other types of deformities (e.g. plagiocephaly). Although these works have shown the potential of 3D photography to identify surgical changes, they do not offer an accurate identification and quantification of local malformations. In addition, most of these results are based on manual processing that makes results subject to human biases and hard to translate into the clinics.

In a proof-of-concept study[18], we showed that 3D photography can quantify significant head shape differences between patients with craniosynostosis and patients with cleft-palate without diagnosed cranial malformations. In the current work, we present a fully automatic, objective, and quantitative framework to evaluate local head shape using 3D photography. First, we created a normative statistical head shape model using a large CT image database of subjects without cranial pathology. Then, we created methods to automatically extract the head shape of a patient from a 3D photograph, and we quantified local head shape abnormalities by comparing the patient's head shape with its projection in the normative statistical model. After showing both quantitatively and qualitatively that 3D photography provides the same quantification of head shape than CT using paired studies, we established normative ranges of our metrics of head shape. Using these metrics, we created classification models that could detect patients with craniosynostosis and identify the fused suture in patients with single suture fusion. Finally, we demonstrated the effective use of this technology to evaluate head shape after surgical treatment to quantify improvements.

Materials and Methods

Data description

Normative population: After approval of our institutional review board, we obtained retrospective head axial CT images from 201 subjects without cranial pathology (age 1.93 ± 1.69 years, range 0-6 years; 89 females and 112 males). The in-plane pixel size of the CT image in our dataset ranged 0.26-0.49 mm, with a slice thickness spacing range of [0.33-5.39] mm. Images were acquired with a variety of CT scanners: General Electric LightSpeed Ultra and LightSpeed Discovery 690 (General Electric, Fairfield, Connecticut, USA), and Philips Brilliance 40 and Brilliance 64 (Philips, Amsterdam, The Netherlands).

Patient population: Retrospective pre-operative CT images with the same specifications as in the normative population were obtained for 214 patients (age 0.77 ± 1.29 years, range 0-6 years; 72 females and 142 males) with craniosynostosis. These include 116 patients with sagittal suture fusion, 46 with coronal suture fusion, 25 with metopic suture fusion, and 27

patients with a different variety of types of craniosynostosis (e.g. multi-suture, pansynostosis).

We also collected retrospectively the pre-operative 3D photographs of 52 patients (age 1.31 ± 1.91 years, range 0-6 years; 19 females and 33 males) with craniosynostosis, including 21 patients with sagittal suture fusion, 16 with coronal suture fusion, 6 with metopic suture fusion and 9 with a variety of types of craniosynostosis. For 34 of these patients (13 female and 21 males), both pre-operative CT images and 3D photographs were available. The 3D photograph was acquired at 17.80 ± 23.55 days after the CT image.

Finally, we also collected retrospectively the post-operative 3D photographs of 18 patients (age at surgery 2.68 ± 3.17 years; 7 females and 11 males) who also had a pre-operative CT image and who underwent cranial vault reconstruction surgery. All surgeries were performed by one of three different neurosurgeons and one of three different plastic surgeons at our institution. The time between the pre-surgical CT image of these patients and surgery was 3.73 ± 3.95 months, and the time between surgery and the post-operative 3D photograph was 34.69 ± 48.69 months.

All 3D photographs were acquired using the 3DMDhead System (3dMD, Atlanta, GA).

Quantification of head shape abnormalities

We used our previously presented algorithms to extract the head shape from CT images [5,18,19] and to label the cranial bones. We created a triangular mesh representing the head and we converted it to signed distance functions to standardize its representation. We used a similar approach[18] to extract the head shape from the 3D photograph of a patient. Since the cranial bones are not visible in 3D photographs, we estimated the location of each cranial bone by projecting bone labels from a reference template onto the patients head shape[18].

Using the head shapes of our subjects without cranial pathology, we created a normative statistical head shape model using PCA[20] as in our previous work modeling cranial bone shapes[5], retaining 75% of the variance in the model. Then, given the head shape of a patient (either obtained from CT or from 3D photography), we calculated its projection on the space of the normative statistical head shape model, allowed identifying the closest normal head shape to that patient. Then, we quantified two shape metrics at each point of the head: (1) malformations, which are the local distances between the patient's head and its matched normal head shape; and (2) curvature discrepancies, which are the local curvature differences.

We tested if our metrics calculated from the CT images were different than the ones obtained from 3D photographs using our patient database with paired CT images and 3D photographs (N=34) and the Wilcoxon signed-rank test. Since the 3D photographs were typically acquired a few weeks after their matched CT images, we compensated for changes caused by natural growth by matching the head size from both modalities at the cranial base using isotropic scaling.

Automatic detection and classification of craniosynostosis

We calculated the average and range of malformations and curvature discrepancies at the area of each cranial bone and suture on the head shapes of our normative population (N=201). We also calculated these metrics from pre-operative CT images (N=214) and 3D photographs (N=52) of our patients with craniosynostosis (N=266). We used these values together with the cephalic index to train a support vector machine classifier[21] to distinguish between patients with and without craniosynostosis, which are machine learning methods that have been used successfully for regression analysis of high-dimensional data in the medical field [5,22,23]. From the probability distribution obtained from cross-validation, we also estimated the power of our classification model.

We trained three additional classifiers to distinguish between patients with sagittal (N=137), coronal (N=62) and metopic (N=31) single suture fusion, similar to previous work quantifying bone shape abnormalities from CT[5]. We did not include patients with fusion of other sutures (i.e. fronto-sphenoidal or lambdoid) because of the low number of patients available. The classification accuracy, sensitivity and specificity were evaluated using cross-validation. As a reference of performance, we compared the results with the methods by Mendoza et al.[5] on the cranial bone shapes from the current CT image dataset using Fisher's exact test.

Post-surgical evaluation of head shapes from 3D photography—We quantified the head shape metrics from the post-surgical 3D photographs of the patients for whom pre-operative CT images were also available (N=18), similar to the pre-operative head shape analysis. Then, we compared the head shape metric values between the pre- and post-operative studies.

Results

Quantification of head shape abnormalities

Tables 1 and 2 show the average head shape metrics obtained for the normative subjects and the patients with craniosynostosis grouped by their fused suture. The malformations and curvature discrepancies on our dataset with paired images were not statistically different between CT and 3D photography (p-values were 0.39 and 0.44, respectively). These results indicate that CT and 3D photography provide the same quantification of head shape. Figures 1 and 2 show the head shape metrics for one example patient with sagittal craniosynostosis from the pre-operative CT image and 3D photograph, respectively.

Automatic detection and classification of craniosynostosis

Our classifier obtained an accuracy of 95.29% (94.74% sensitivity, 96.02% specificity) for the detection of patients with craniosynostosis from their metrics of head shape, with a power of 94% for a 95% confidence. In addition, we obtained accuracies of 99.57% (100.00% sensitivity, 98.92% specificity), 99.57% (100.00% sensitivity, 99.40% specificity), and 99.13% (93.55% sensitivity, 100.00% specificity) identifying the suture fused in patients with sagittal, coronal, and metopic single suture fusion, respectively. Finally, the Fisher's exact test concluded that the classification obtained with the proposed method was not

independent from previous methods analyzing cranial bone shapes from CT images [5] ($p<0.001$).

Post-surgical evaluation of head shapes from 3D photography—We calculated our head shape metrics on the pre-surgical head shapes from CT images and the post-surgical shapes from 3D photography for our dataset of 18 patients. The average values of our metrics at each cranial bone area is presented in Tables 3 and 4 in the pre- and post-surgical head shapes, respectively. In absolute value, we obtained average malformations of 3.24 ± 1.09 mm in the pre-surgical shapes of these patients, and 1.90 ± 0.51 mm in the post-surgical shapes, which represented a reduction of malformations of 41.36% ($p<0.001$ using a paired Wilcoxon signed rank-sum test). We obtained average curvature discrepancies with respect to the normative statistical model in the pre-surgical head shapes of 0.62 ± 0.10 mm^{-1} and in the post-surgical shapes of 0.56 ± 0.06 mm^{-1}, which represents a reduction of 9.68% ($p=0.03$). Finally, we used our previously trained classifier to determine whether the head shapes of these patients were normal or abnormal. Our classifier identified correctly that all pre-operative head shapes corresponded to patients with craniosynostosis. Interestingly, it also provided the result that all post-surgical head shapes were not in normative ranges despite the significant reduction of malformations after surgery. As a visual example, we show in Figure 3 the pre- and post-surgical head shape metrics quantified for one patient with bicoronal craniosynostosis, where we can observe a significant reduction of abnormalities after surgical treatment.

Discussion

Three-dimensional photography is a cheap and fast imaging modality that does not involve risks for the patients. However, current clinical approach has not benefitted yet from automatic and quantitative methods to evaluate accurately local head shape abnormalities and their surgical correction. In this work, we have presented a fully automated and objective method to quantify local head malformations, and we have used them to evaluate patients with craniosynostosis both pre- and post- surgically.

We have demonstrated that head shape metrics calculated from 3D photography are as accurate as those calculated from CT images using a dataset of patients with paired images. Tables 1 and 2 show in a quantitative and objective way that patients with sagittal suture fusion present underdeveloped and flatter head shapes at the parietal areas, and overdeveloped heads in the frontal and occipital areas. Patients with coronal craniosynostosis present underdeveloped and flatter head shapes at the areas close to the fused sutures. Patients with metopic craniosynostosis present a typical high curvature at the area of the metopic suture and flatter frontal bone areas. These metrics were objectively computed using a dataset of normative head shapes and represent an intuitive and reproducible interpretation of head malformations, as illustrated in Figures 1 and 2 with an example of a patient with sagittal craniosynostosis.

We used our metrics to detect patients with craniosynostosis with over 95% accuracy and identify what suture is fused in patients with sagittal, coronal, and metopic single suture fusion with 99% accuracy. Although it is known that patients with the same type of

craniosynostosis present similar abnormal patterns of head shape, we have shown that these abnormal phenotypes can be quantified accurately and locally using intuitive metrics of head shape.

We have also demonstrated the potential of 3D photography and our quantitative framework to objectively evaluate the surgical outcome for patients with craniosynostosis. We quantified head shape abnormalities for a dataset of patients with pre-operative CT images and post-surgical 3D photographs and we presented the results in Tables 3 and 4. Our methods showed a significant reduction of cranial shape abnormalities as a result of surgical correction.

Interestingly, our results also indicated that none of the patients had normative head shapes after treatment. This can be intuitively concluded by comparing the post-surgical malformations and curvature discrepancies from Tables 3 and 4, with the normative values presented in Tables 1 and 2. The post-surgical head shapes of our patients generally present positive malformations higher than the normative ranges. As positive malformations represent overdevelopment, these results are related to the overcorrection that is typically applied during surgery to create volume for the brain to resume a normal growth. In addition, the local constraints imposed by suture fusion before surgical treatment often causes a compensatory overgrowth in other areas of the head, which explains higher malformation values at areas of the head without fusion constraints. On the other hand, although curvature discrepancies with respect to the normative statistical model were significantly improved during surgery for these patients, our quantitative results showed that these improvements did not create bone curvature within normal ranges. Current surgical approach to cranial vault reconstruction is guided by the expert assessment by the surgeons of the balance between the invasiveness of the surgery, the constraints imposed by bone mechanics, and the target surgical outcome based on the observed degree of head malformations, which can be very severe before surgery. Hence, although the abnormalities were significantly reduced, a completely normal head shape is rarely achieved during surgery.

The limitations of current study are related to the database available. Our normative and patient databases only included patients up to 6 years of age. Although most patients with craniosynostosis are diagnosed within the first year of life, there are some patients who develop craniosynostosis later in their lives, which is more challenging to diagnose because of the lower degree of malformations and symptoms observed. In addition, although we have successfully used our methods to automatically detect the fused suture in patients with sagittal, coronal or metopic suture fusion, we could not demonstrate suture fusion detection on patients with other types of craniosynostosis with lower incidence rates (e.g. lambdoid, fronto-sphenoidal…) because of low data availability.

Our study, however, has successfully shown that the presented methodology can quantify head shape and identify local abnormalities in patients with craniosynostosis. We have also shown its potential to evaluate quantitatively the outcome of surgical treatment at the clinics without exposing children to unnecessary radiation. On the other hand, our quantitative framework provides the necessary tools to study head malformations longitudinally at a low

cost and without any risk for the patients. Hence, the presented technology provides a powerful tool to detect relapses or development abnormalities before patients become symptomatic. Finally, in addition to the increasing use at the clinics of 3D photography scanners, modern mobile phones are building camera capabilities to create three-dimensional reconstructions of faces and heads. The presented quantitative methods together with new mobile technologies could enable an accurate and objective quantification of head abnormalities in clinics where 3D scanners are not available.

Conclusion

Quantitative head shape analysis and 3D photography provide accurate, automatic, and objective tools to screen patients for head shape abnormalities. These tools are fast, cheap, and avoid exposing children to radiation or sedation for clinical assessment. Our quantitative framework also provides the tools to objectively evaluate treatment outcomes, which is essential to optimize and evaluate surgical procedures, and to detect and even prevent possible relapses.

Acknowledgments

Financial Disclosure Statement:

This work was partly funded by the Eunice Kennedy Shriver National Institute of Child Health and Human Development (National Institutes of Health) under grant R42HD081712. The authors have no financial interests related to this work.

References

1. Lajeunie E, Le Merrer M, Bonaïti-Pellie C, Marchac D, Renier D. Genetic study of nonsyndromic coronal craniosynostosis. Am J Med Genet. 1995;55(4):500–504. doi:10.1002/ajmg.1320550422. [PubMed: 7762595]
2. Wilkie AOM. Epidemiology and genetics of craniosynostosis. Am J Med Genet. 2000;90(1):82–83. doi:10.1002/(SICI)1096-8628(20000103)90:1<82::AID-AJMG15>3.0.CO;2-5. [PubMed: 10602123]
3. Johnson D, Wilkie AOM. Craniosynostosis. Eur J Hum Genet. 2011;19(4):369–376. doi:10.1038/ejhg.2010.235. [PubMed: 21248745]
4. Kirmi O, Lo SJ, Johnson D, Anslow P. Craniosynostosis: A Radiological and Surgical Perspective. Semin Ultrasound, CT MRI. 2009;30(6):492–512. doi:10.1053/j.sult.2009.08.002.
5. Mendoza CS, Safdar N, Okada K, Myers E, Rogers GF, Linguraru MG. Personalized assessment of craniosynostosis via statistical shape modeling. Med Image Anal. 2014;18(4):635–646. doi:10.1016/j.media.2014.02.008. [PubMed: 24713202]
6. Breakey RWF, Knoops PGM, Borghi A, et al. Intracranial Volume and Head Circumference in Children with Unoperated Syndromic Craniosynostosis. Plast Reconstr Surg. 2018;142(5):708e–717e. doi:10.1097/PRS.0000000000004843.
7. Morgan C, McGowan P, Herwitker S, Hart AE, Turner MA. Postnatal Head Growth in Preterm Infants: A Randomized Controlled Parenteral Nutrition Study. Pediatrics. 2014. doi:10.1542/peds.2013-2207.
8. Thakkar PA, Yagnik K, Parmar NT, Das RR, Thakkar UP. Observer variability in head circumference measurement using routine versus non-stretchable tapes in children. J Nepal Paediatr Soc. 2018. doi:10.3126/jnps.v37i3.19556.
9. Fearon JA, Ditthakasem K, Herbert M, Kolar J. An Appraisal of the Cephalic Index in Sagittal Craniosynostosis, and the Unseen Third Dimension. Plast Reconstr Surg. 2017;140(1):138–145. doi:10.1097/PRS.0000000000003422. [PubMed: 28654600]

10. Morritt DG, Yeh F-JJ, Wall SA, Richards PG, Jayamohan J, Johnson D. Management of Isolated Sagittal Synostosis in the Absence of Scaphocephaly: A Series of Eight Cases. Plast Reconstr Surg. 2010;126(2):572–580. doi:10.1097/PRS.0b013e3181e09533. [PubMed: 20679839]
11. Sgouros S, Hockley AD, Goldin JH, Wake MJ, Natarajan K. Intracranial volume change in craniosynostosis. J Neurosurg. 1999;91(4):617–625. doi:10.3171/jns.1999.91.4.0617. [PubMed: 10507384]
12. Hill CA, Vaddi S, Moffitt A, et al. Intracranial volume and whole brain volume in infants with unicoronal craniosynostosis. Cleft Palate Craniofac J. 2011;48(4):394–398. doi:10.1597/10-051. [PubMed: 20815706]
13. Gault DT, Renier D, Marchac D, Ackland FM, Jones BM. Intracranial Volume in Children With Craniosynostosis. J Craniofac Surg. 1990;1(1). https://journals.lww.com/jcraniofacialsurgery/Fulltext/1990/01000/Intracranial_Volume_in_Children_With.3.aspx.
14. Porras AR, Paniagua B, Ensel S, et al. Locally Affine Diffeomorphic Surface Registration and Its Application to Surgical Planning of Fronto-Orbital Advancement. IEEE Trans Med Imaging. 2018;37(7):1690–1700. doi:10.1109/TMI.2018.2816402. [PubMed: 29969419]
15. Tenhagen M, Bruse JL, Rodriguez-Florez N, et al. Three-Dimensional Handheld Scanning to Quantify Head-Shape Changes in Spring-Assisted Surgery for Sagittal Craniosynostosis. J Craniofac Surg. 2016;27(8):2117–2123. doi:10.1097/SCS.0000000000003108. [PubMed: 28005766]
16. Rodriguez-Florez N, Göktekin ÖK, Bruse JL, et al. Quantifying the effect of corrective surgery for trigonocephaly: A non-invasive, non-ionizing method using three-dimensional handheld scanning and statistical shape modelling. J Cranio-Maxillofacial Surg. 2017;45(3):387–394. doi:10.1016/j.jcms.2017.01.002.
17. Meulstee JW, Verhamme LM, Borstlap WA, et al. A new method for three-dimensional evaluation of the cranial shape and the automatic identification of craniosynostosis using 3D stereophotogrammetry. Int J Oral Maxillofac Surg. 2017;46(7):819–826. doi:10.1016/j.ijom.2017.03.017. [PubMed: 28392059]
18. Tu L, Porras AR, Oh A, et al. Radiation-free quantification of head malformations in craniosynostosis patients from 3D photography In: Mori K, Petrick N, eds. Medical Imaging 2018: Computer-Aided Diagnosis. Vol 10575 SPIE; 2018:65–70. doi:10.1117/12.2295374.
19. Tu L, Porras AR, Ensel S, et al. Intracranial Volume Quantification from 3D Photography In: Computer Assisted and Robotic Endoscopy and Clinical Image-Based Procedures. CARE 2017, CLIP 2017. Vol 10550 Springer, Cham; 2017:116–123. doi:10.1007/978-3-319-67543-5_11. [PubMed: 29167840]
20. Pearson K LIII. On lines and planes of closest fit to systems of points in space. Philos Mag Ser 6. 1901;2(11):559–572. doi:10.1080/14786440109462720.
21. Cortes C, Vapnik V. Support-vector networks. Mach Learn. 1995;20(3):273–297. doi:10.1007/BF00994018.
22. Cerrolaza JJ, Porras AR, Mansoor A, Zhao Q, Summar M, Linguraru MG. Identification of dysmorphic syndromes using landmark-specific local texture descriptors. 2016 IEEE 13th Int Symp Biomed Imaging April 2016:1080–1083. doi:10.1109/ISBI.2016.7493453.
23. Blum ES, Porras AR, Biggs E, et al. Early Detection of Ureteropelvic Junction Obstruction Using Signal Analysis and Machine Learning: A Dynamic Solution to a Dynamic Problem. J Urol. 2018;199(3):847–852. doi:10.1016/j.juro.2017.09.147. [PubMed: 29066360]

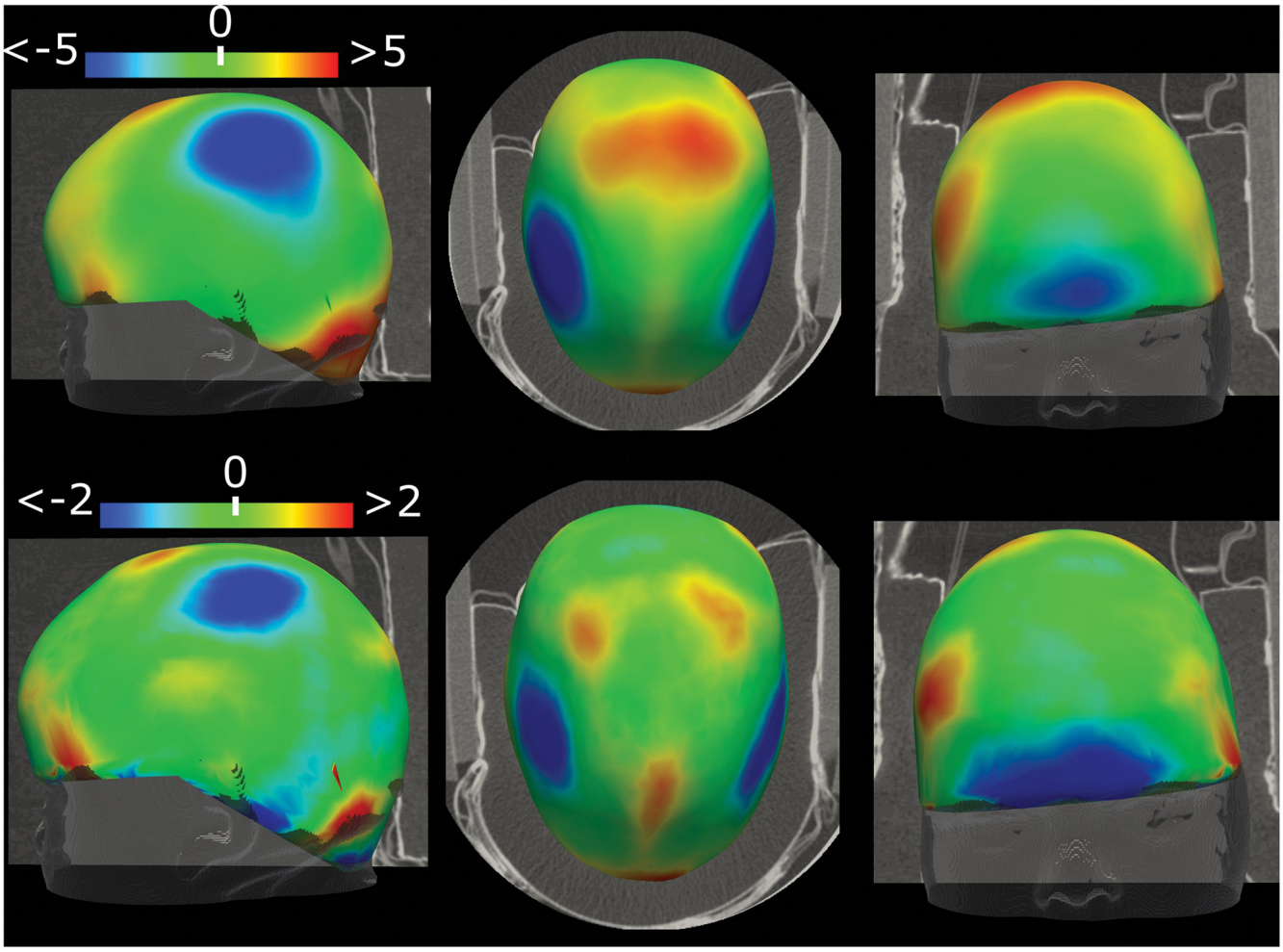

Figure 1.

Head shape metrics calculated for one example patient with sagittal craniosynostosis from the pre-operative CT image: (above) local malformations in mm and (below) curvature discrepancies in mm^{-1}. Positive malformations represent overdevelopment and negative values represent underdevelopment. Positive curvature discrepancies represent sharper areas than the normative model, while negative values represent flatter areas.

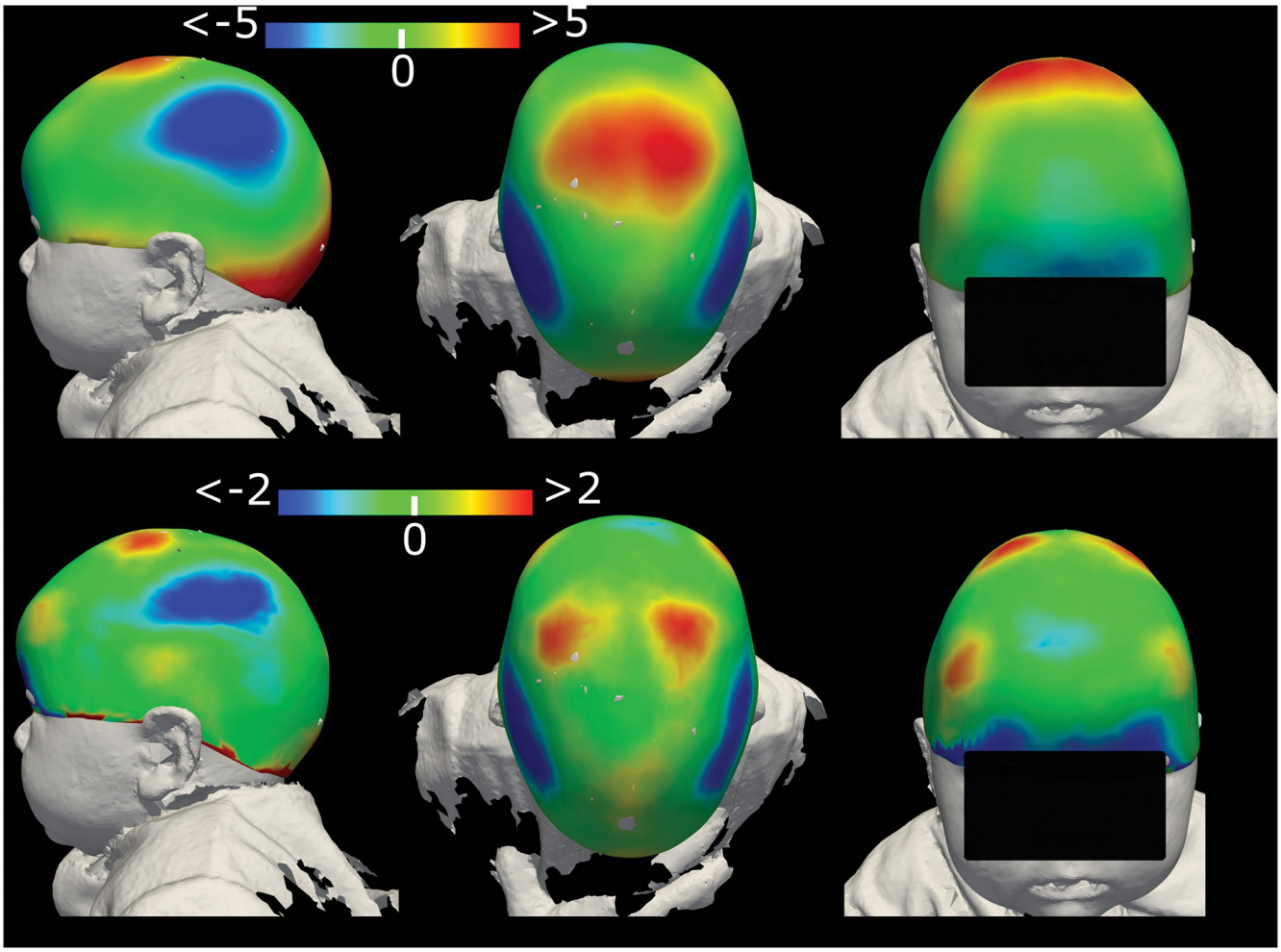

Figure 2.

Head shape metrics calculated from 3D photograph of the patient with sagittal craniosynostosis shown in Figure 1: (above) local malformations in mm and (below) curvature discrepancies in mm^{-1}. Positive malformations represent overdevelopment and negative values represent underdevelopment. Positive curvature discrepancies represent shaper areas than the normative model, while negative values represent flatter areas.

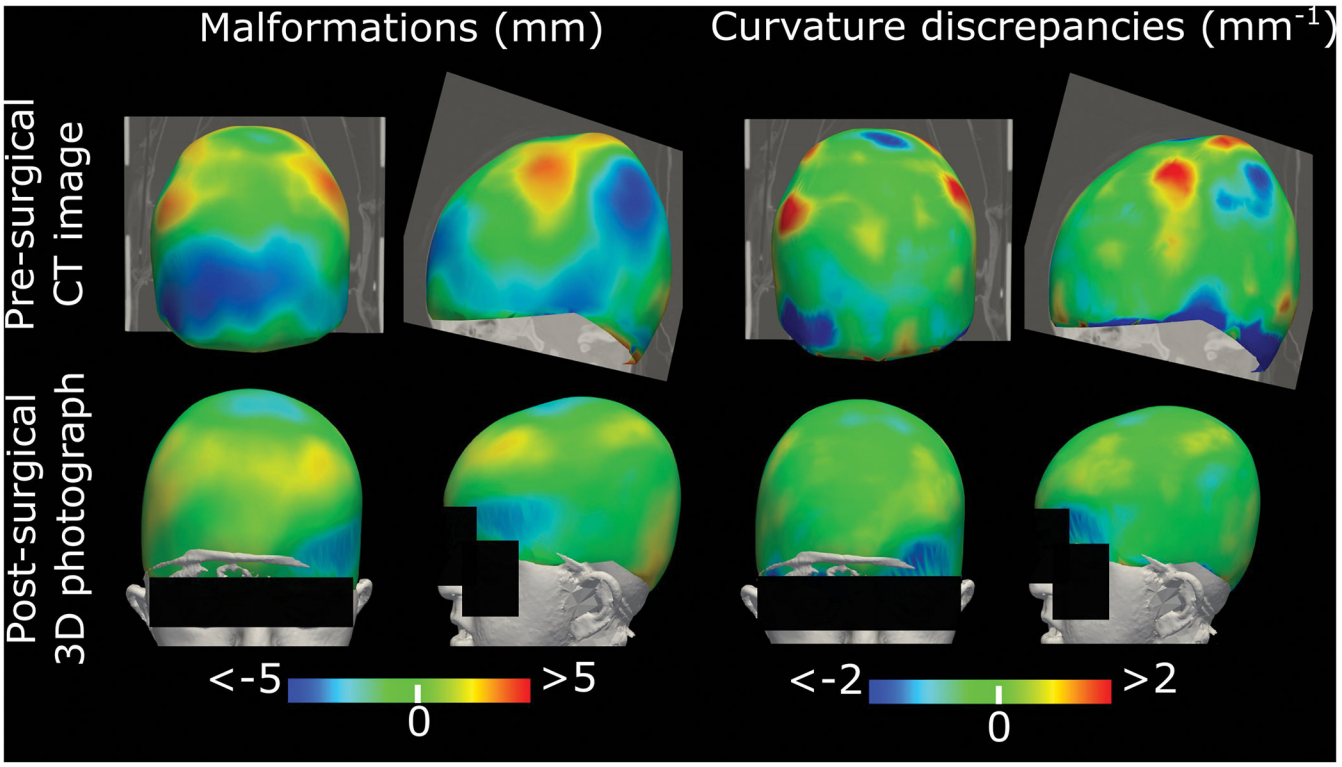

Figure 3.

Example of head shape metrics on the pre- (from CT) and post-surgical head shape (from 3D photography) of a patient with bicoronal craniosynostosis. Frontal and lateral views of the (above) local malformations in mm and (below) curvature discrepancies in mm^{-1}. Positive malformations represent overdevelopment and negative values represent underdevelopment. Positive curvature discrepancies represent shaper areas than the normative model, while negative values represent flatter areas.

Table 1.

Ranges of malformations in mm in our normative subjects, and in patients with sagittal, left (L.) coronal, right (R.) coronal, bicoronal and metopic craniosynostosis at the area of each bone and suture. Positive values represent overdevelopment compared to the normative model, and negative values represent underdevelopment. For visual guidance, average malformations were color coded. Blue represents negative values and red positive values. The scale of the magnitude is indicated by the intensity of colors.

Bones	Left parietal			Right parietal			Left frontal			Right frontal			Occipital		
	Avg	Max	Min	Avg	Max	Min	Avg	Max	Min	Avg	Max	Min	Avg	Max	Min
Normative	0.74	2.71	−0.99	0.72	2.81	−1.06	0.80	2.32	−0.66	0.80	2.28	−0.57	0.80	2.69	−0.95
Sagittal	−0.85	4.01	−4.40	−0.67	4.08	−4.05	1.57	4.34	−2.27	2.14	4.80	−1.85	2.46	5.82	−0.92
L. Coronal	0.46	3.62	−2.38	0.67	3.34	−1.83	−0.55	1.99	−3.43	1.27	2.70	−0.78	−0.20	2.51	−2.17
R. Coronal	1.04	3.93	−2.18	0.37	3.69	−2.44	0.74	3.06	−2.36	0.05	3.13	−3.27	0.02	3.20	−2.76
Bicoronal	0.48	5.78	−3.33	0.79	5.49	−3.09	−1.41	3.92	−7.75	−1.42	4.14	−7.83	−0.09	4.57	−3.72
Metopic	0.77	3.22	−1.44	0.81	3.07	−1.48	0.00	3.45	−2.23	0.10	3.23	−2.13	0.14	2.79	−1.99

Sutures	Left coronal			Right coronal			Metopic			Sagittal		
	Avg	Max	Min	Avg	Max	Min	Avg	Max	Min	Avg	Max	Min
Normative	0.71	1.87	−0.41	0.70	1.86	−0.39	0.74	2.06	−0.52	0.57	1.76	−0.60
Sagittal	0.99	3.97	−1.66	1.60	4.29	−1.32	1.51	4.08	−1.56	0.85	4.02	−1.23
L. Coronal	0.29	2.48	−1.72	0.90	2.19	−0.89	0.54	1.95	−1.83	0.43	2.29	−1.27
R. Coronal	1.28	3.02	−1.04	0.96	3.43	−1.26	0.10	2.23	−2.85	0.69	2.85	−1.30
Bicoronal	1.94	5.16	−1.20	1.76	4.84	−1.66	−2.07	3.61	−8.04	1.20	3.88	−1.53
Metopic	0.40	1.77	−1.36	0.61	2.10	−1.43	1.57	4.24	−0.54	0.94	2.62	−0.47

Table 2.

Ranges of curvature discrepancies in mm^{-1} in our normative subjects, and in patients with sagittal, left coronal, right coronal, bicoronal and metopic craniosynostosis at the area of each bone and suture. Positive values represent shaper areas than the normative model and negative values represent flatter areas. For visual guidance, average curvature discrepancies were color coded. Blue represents negative values and red positive values. The scale of the magnitude is indicated by the intensity of colors.

Bones	Left parietal			Right parietal			Left frontal			Right frontal			Occipital		
	Avg	Max	Min	Avg	Max	Min	Avg	Max	Min	Avg	Max	Min	Avg	Max	Min
Normative	−0.05	1.39	−1.30	−0.05	1.63	−1.27	−0.05	1.31	−1.19	−0.05	1.02	−1.19	−0.18	1.28	−1.74
Sagittal	−0.23	2.08	−2.03	−0.19	2.13	−1.95	0.15	1.82	−1.88	0.22	1.76	−1.80	0.09	2.21	−1.29
L. Coronal	−0.07	1.98	−1.68	−0.02	1.48	−1.31	−0.36	1.18	−2.52	0.08	1.54	−1.28	−0.30	1.71	−1.97
R. Coronal	0.01	1.80	−1.36	−0.13	2.42	−2.00	0.02	1.73	−1.56	−0.21	1.42	−2.34	−0.24	1.34	−2.19
Bicoronal	−0.14	1.64	−1.79	−0.08	2.12	−1.90	−0.20	1.60	−2.72	−0.11	1.60	−2.33	−0.20	2.70	−2.11
Metopic	−0.02	1.46	−1.74	0.01	1.36	−1.44	−0.42	1.75	−2.08	−0.44	1.22	−2.01	−0.16	1.38	−1.90

Sutures	Left coronal			Right coronal			Metopic			Sagittal		
	Avg	Max	Min	Avg	Max	Min	Avg	Max	Min	Avg	Max	Min
Normative	−0.04	0.86	−0.73	−0.04	0.87	−0.72	−0.05	0.80	−1.06	−0.04	0.73	−0.78
Sagittal	0.10	1.49	−0.98	0.17	1.49	−0.90	−0.20	0.96	−1.76	−0.01	1.28	−1.06
L. Coronal	−0.12	1.68	−1.31	0.12	0.88	−0.73	−0.02	0.99	−1.62	−0.09	0.85	−1.01
R. Coronal	0.17	1.15	−0.80	−0.01	1.26	−1.75	−0.17	1.00	−1.72	−0.01	1.02	−0.96
Bicoronal	0.38	1.77	−0.85	0.39	1.70	−0.82	−0.21	1.17	−2.05	0.18	1.25	−0.86
Metopic	−0.02	1.30	−1.13	0.01	1.09	−1.11	0.35	2.01	−0.91	0.08	1.12	−0.67

Table 3.

Average malformations in mm at the area of each cranial bone (LP: left parietal; RP: right parietal; LF: left frontal; RF: right frontal; O: occipital) in the pre- and post-surgical head shapes of 18 patients with craniosynostosis. Positive values represent overdevelopment compared to the normative model, and negative values represent underdevelopment. For visual guidance, average malformations were color coded. Blue represents negative values and red positive values. The scale of the magnitude is indicated by the intensity of colors.

#	Suture fusion	Pre-surgical					Post-surgical				
		LP	RP	LF	RF	O	LP	RP	LF	RF	O
1	Bicoronal	1.41	0.96	−3.95	−2.13	−2.78	1.19	0.77	0.63	1.72	−0.81
2	Left coronal	1.88	2.38	−2.56	−0.06	−4.40	1.00	0.80	0.07	1.27	−1.64
3	Left coronal + lambdoid	−1.47	1.14	−3.64	−6.44	−3.89	0.47	1.43	−0.58	−0.54	0.88
4	Left fronto-sphenoidal	0.80	0.86	−2.31	1.4	−1.50	0.73	0.39	−0.36	1.39	−1.18
5	Metopic	2.11	2.26	0.19	4.61	−1.60	1.41	0.98	−0.70	0.48	0.04
6	Pansynostosis	2.57	2.50	0.49	−4.5	−1.69	0.57	0.09	−0.30	2.07	0.27
7	Pansynostosis	−0.87	−0.63	−6.91	3.07	−7.98	1.37	1.46	1.08	1.66	−2.15
8	Pansynostosis	−1.04	−1.25	0.26	0.28	2.31	−0.13	−0.84	0.58	2.44	2.94
9	Pansynostosis	−0.94	−0.75	−0.57	5.07	0.76	−0.47	−0.40	0.35	1.44	2.65
10	Pansynostosis	0.72	0.86	−1.81	0.39	−0.73	0.95	0.93	−0.44	0.96	−1.40
11	Sagittal	−3.87	−5.08	2.25	3.49	5.70	−0.67	−0.40	2.41	2.50	3.44
12	Sagittal	−1.49	−1.42	5.79	−0.31	3.08	0.78	1.07	0.11	2.60	1.09
13	Sagittal	−3.27	−2.40	4.23	2.34	3.57	0.22	0.46	1.49	3.51	1.15
14	Sagittal	−1.44	−1.41	3.00	4.91	4.07	0.26	−0.09	1.09	3.31	3.45
15	Sagittal	−1.34	−1.27	5.33	1.18	2.95	1.61	1.88	1.98	0.93	1.19
16	Sagittal	−0.85	−1.26	1.51	−1.4	1.55	0.93	0.46	−0.36	−0.07	0.35
17	Sagittal	−4.24	−5.44	1.37	−2.57	5.55	0.86	1.24	0.24	1.01	−0.13
18	Sagittal + right lambdoid	−0.93	−5.65	1.72	1.5	6.88	0.26	−0.40	2.27	4.34	5.02

Table 4.

Average curvature discrepancies with respect to the normative statistical model in mm^{-1} at the are of each cranial bone (LP: left parietal; RP: right parietal; LF: left frontal; RF: right frontal; O: occipital) in the pre- and post-surgical head shapes of 18 patients with craniosynostosis. Positive values represent shaper areas than the normative model and negative values represent flatter areas. For visual guidance, average curvature discrepancies were color coded. Blue represents negative values and red positive values. The scale of the magnitude is indicated by the intensity of colors.

#	Suture fusion	Pre-surgical					Post-surgical				
		LP	RP	LF	RF	O	LP	RP	LF	RF	O
1	Bicoronal	0.09	−0.05	−0.43	−0.41	−0.23	−0.05	−0.10	−0.15	−0.09	−0.24
2	Left coronal	−0.05	0.09	−0.29	−0.08	−0.91	−0.17	0.03	−0.20	−0.01	−0.33
3	Left coronal + lambdoid	−0.30	0.04	−0.55	−0.18	−0.97	−0.34	−0.03	−0.24	−0.15	−0.08
4	Left fronto-sphenoidal	−0.02	0.07	−0.29	−0.15	−0.50	−0.13	0.00	−0.24	0.06	−0.41
5	Metopic	0.04	−0.01	−0.48	−0.72	0.19	−0.11	−0.10	−0.32	−0.16	−0.09
6	Pansynostosis	0.14	0.07	−0.03	−0.06	−0.21	0.05	−0.01	−0.16	0.31	0.13
7	Pansynostosis	−0.01	−0.07	−0.62	−0.59	−0.98	0.01	−0.07	0.01	−0.06	−0.32
8	Pansynostosis	−0.10	−0.14	−0.09	−0.01	0.01	−0.03	−0.02	−0.20	0.15	0.11
9	Pansynostosis	−0.07	−0.03	−0.20	−0.22	−0.10	−0.11	−0.14	−0.11	−0.07	0.32
10	Pansynostosis	0.00	−0.03	−0.43	−0.42	−0.32	−0.03	0.02	−0.15	0.05	−0.30
11	Sagittal	−0.19	−0.31	0.10	0.21	−0.05	−0.02	0.04	0.20	0.22	0.32
12	Sagittal	−0.28	−0.24	0.21	0.22	0.08	0.09	0.10	−0.08	0.25	−0.14
13	Sagittal	−0.52	−0.36	0.21	0.21	−0.13	−0.02	−0.06	0.03	0.26	−0.04
14	Sagittal	−0.20	−0.21	0.16	0.04	0.19	0.06	−0.05	0.02	0.29	0.29
15	Sagittal	−0.10	−0.19	0.13	0.17	0.05	0.04	0.13	0.18	0.14	0.22
16	Sagittal	−0.13	−0.26	−0.21	−0.37	−0.22	0.01	−0.07	−0.20	−0.05	−0.11
17	Sagittal	−0.15	−0.31	0.07	0.15	−0.02	0.02	0.17	−0.12	0.02	−0.10
18	Sagittal + right lambdoid	−0.34	−0.84	0.11	0.06	0.01	−0.14	−0.24	0.13	0.11	0.58